ORIGINAL ARTICLE

circ_0007385 served as competing endogenous RNA for miR-519d-3p to suppress malignant behaviors and cisplatin resistance of non-small cell lung cancer cells

Yancheng Ye[1], Liangcun Zhao[1], Qingke Li[2], Caixia Xi[3], Yinghong Li[4] & Zhengguo Li[3] (iD)

1 Department of Pharmacy, Gansu Wuwei Tumor Hospital, Wuwei, China
2 Department of Laboratory medicine, Gansu Wuwei Tumor Hospital, Wuwei, China
3 Department of Respiratory Medicine, Gansu Wuwei Tumor Hospital, Wuwei, China
4 Department of Integrated Traditional Chinese and Western Medicine, Gansu Wuwei Tumor Hospital, Wuwei, China

Abstract

Background: Circular RNAs (circRNAs) have been closely implicated in competing endogenous RNA (ceRNA) network among human cancers including non-small cell lung cancer (NSCLC). However, the role of most circRNAs in NSCLC remains to be determined. Here, we aimed to investigate the role of hsa_circ_0007385 (circ_0007385) in NSCLC cells.

Methods: Expression of hsa_circ_0007385 (circ_0007385), miRNA (miR)-519d-5p and high-mobility group box 1 (HMGB1) was measured by real-time quantitative PCR and western blotting. Functional experiments were evaluated by cell counting kit (CCK)-8, flow cytometry, fluorescein active caspase-3 staining kit, transwell assays, western blotting, and xenograft experiment. The relationship among circ_0007385,miR-519d-5p and HMGB1 was testified by dual-luciferase reporter assay. Kaplan-Meiersurvival curve identified overall survival in NSCLC patients.

Results: circ_0007385 expression was higher in NSCLC tissues and cell lines, and was associated with poor overall survival. Silencing circ_0007385 could suppress cell proliferation, migration and invasion in A549 and H1975 cells, as well as cisplatin (DDP) resistance. Moreover, circ_0007385 silence retarded tumor growth of A549 cells in vivo. Molecularly, there was a direct interaction between miR-519d-3p and either circ_0007385 or HMGB1; expression of miR-519d-3p was downregulated in NSCLC tumors in a circ_0007385-correlated manner, and circ_0007385 could indirectly regulate HMGB1 via miR-519d-3p. Functionally, both inhibiting miR-519d-3p and restoring HMGB1 could overturn the suppressive effect of circ_0007385 knockdown on cell proliferation, migration, invasion, and DDP resistance.

Conclusions: Collectively, circ_0007385 deletion could function anti-tumor role in NSCLC by suppressing malignant behaviors and DDP resistance in vitro and in vivo via circ_0007385/miR-519d-3p/HMGB1 axis. These outcomes might enhance our understanding of the molecular mechanisms underlying the malignant progression of NSCLC.

Key points

Significant findings of the study:
- circ_0007385 was upregulated in NSCLC tissues and cells, and was associated with poor overall survival.

- Silenced circ_0007385 suppressed NSCLC cell proliferation, migration, invasion, and DDP resistance in vitro, and tumor growth in vivo.
- circ_0007385 was upregulated in NSCLC tissues and cells, and was associated with poor overall survival.

What this study adds:

- miR-519d-3p could directly interact with circ_0007385 and HMGB1 in NSCLC cells.
- A promising circ_0007385/miR-519d-3p/HMGB1 regulatory pathway was determined in NSCLC cells.

Introduction

Lung cancer is one of the leading cancers both in morbidity and mortality worldwide,[1] and the overwhelming subtype of lung cancers representing 85% of cases is non-small cell lung cancer (NSCLC).[2] Lung cancers in particular have been a major public health problem in China.[3] In terms of treatment strategy of lung cancers, surgical resection, platinum-based dual chemotherapy and target therapy are the first-line approaches.[4] However, the long time overall survival of patients with NSCLC is only about 18%,[5] and is still closely related to the stage. In addition, there are still many clinical challenges in NSCLC, including early diagnosis.[6] Cisplatin (DDP), the first metal-based anticancer drug, is widely used in solid cancers including lung cancer[7]; however, DDP resistance has been reported to occur in approximately 63% of NSCLC patients.[8]

Circular RNAs (circRNAs) are a class of endogenous, covalently closed RNAs produced from 'back-splicing' of primary transcripts.[9, 10] Compared with linear RNAs, circRNAs are more stable in vivo over an extended period.[11] CircRNAs are deemed to be diagnostic and prognostic biomarkers in lung cancers,[3] including NSCLC.[12] Functionally, progress in research on the role of circRNAs has also been highlighted in lung cancers.[13, 14] In particular, circRNAs are able to modulate chemoresistance in lung cancers.[15]

It has been well documented that circRNAs can serve as competitive endogenous RNAs (ceRNAs) to inhibit cellular function,[16] and ceRNAs interplay has evolved in the pathogenesis of human cancers including lung cancer.[17] MicroRNAs (miRNAs) are a class of small, linear noncoding RNAs. Recently, miRNA (miR)-519d-3p was found to be downregulated in 97.1% of tissues of NSCLC patients.[18] However, the role of miR-519d-3p is still unclear in NSCLC cells.

The hsa_circ_0007385 (circ_0007385) is derived from host gene MEMO1, and has been declared to be upregulated in NSCLC tissues and cells.[19] In this study, we intended to determine the role of circ_0007385 in malignant behaviors and DDP resistance of NSCLC cells.

Furthermore, the cross-talk among circ_0007385, miR-519d-3p and high-mobility group box 1 (HMGB1) was revealed. HMGB1 is a potential biomarker and therapeutic target for multiple cancers,[20] including lung cancer.[21, 22]

Methods

Tissue sample collection

A cohort of 75 NSCLC patients were recruited at Gansu Wuwei Tumor Hospital, and the fresh tumor tissues and adjacent normal tissues (≥5 cm from tumor margin) were collected during the radical operation after written consent was received from each patient. These patients experienced no systemic chemotherapy or radiotherapy prior to surgery, and the tumor nodes metastasis (TNM) stage was classified according to the American Joint Committee on Cancer lung cancer staging system (eighth edition). The tissue samples were snap-frozen in liquid nitrogen. This study was approved by the Ethics Committee of Gansu Wuwei Tumor Hospital.

Cell culture

Human NSCLC cell lines including A549 (CRM-CCL-185), HCC827 (CRL-2868), H1975 (CRL-5908), and H2342 (CRL-5941) were from the American Type Culture Collection (Manassas, VA, USA), and a normal bronchial epithelial cell line 16HBE (SCC150) was from Millipore (Billerica, MA, USA). The NSCLC cells were maintained in RPMI 1640 (Hyclone, Logan, UT, USA), and 16HBE cells were in DMEM (HyClone). All the cells were incubated in 10% fetal bovine serum (FBS; HyClone) at 37°C with 5% CO_2.

Real-time quantitative PCR (RT-qPCR)

Total RNA in tissues and cell lines was extracted using TRIzol reagent (Invitrogen, Carlsbad, CA, USA) in line with the instructions, and an aliquot of RNA sample (1 μg) was used to synthesize cDNA using RevertAid First-Strand cDNA Synthesis kit (Thermo Fisher Scientific, Foster City,

CA, USA). The RT-qPCR was performed using cDNA, primers and SYBR Green Mix (Thermo Fisher Scientific) on Applied Biosystems 7900 (Thermo Fisher Scientific). The primers were target circ_0007385 (5′-CGTGACCCAG AAGTGCGTTCACA-3′, 5′-TGGGGGTGTATCAGTCTTT GGTT-3′),[18] miR-519d-3p (5′-TCCGAGTGAGATTTCCC TC-3′ and 5′-GTGCAGGGTCCGAGGT-3′), HMGB1 (5′-CTTCTTGAGGGGGAAGCTAGT-3′ and 5′-TTTTGGATG TTCAGTTATGG-3′), glyceraldehyde-phosphate dehydrogenase (GAPDH; 5′-GTGGACATCCGCAAAGAC-3′ and 5′-AAAGGGTGTAACGCAACTA-3′), and U6 (5′-TCCGA TCGTGAAGCGTTC-3′ and 5′-GTGCAGGGTCCGAG GT-3′). GAPDH was used as an endogenous control for circ_0007385 and HMGB1, and U6 was for miR-519d-3p. The relative expression level was calculated using the 2 (-Delta Delta C(T)) method,[23] and every reaction group was repeated in at least four wells.

Cell transfection

The short hairpin RNA (shRNA) targeting circ_0007385 (sh-circ; 5′-AAUAGAACACUUACUACUAAUCUGdTdT-3′ and 3′-dTdTAUUCCCUAGCCCUUCGAGUGTT-5′),[18] miR-519d-3p mimic (5′-CAAAGUGCCUCCCUUUAGAG UG-3′), and miR-519d-3p inhibitor (anti-miR-519d-3p; 5′-CACUCUAAAGGGAGGCACUUUG-3′) were chemically synthesized by Songon Biotech (Shanghai, China), as well as the negative controls. The overexpression vector of HMGB1 was constructed using pEEGFP-C1 (Clontech, Mountain View, CA, USA). For transfection, A549 and H1975 cells were passaged in a six-well plate at a density of 2×10^5 cells/well, and vectors (2 μg) and small RNAs (40 nM) were transfected into cells using Lipofectamine 3000 reagent (Invitrogen) according to the manufacturer's instruction. After transfection for 48 hours, the transfected cells were collected for RT-qPCR and western blotting analysis.

Cell counting kit (CCK)-8 for cell viability and half maximal inhibitory concentration (IC50) of DDP

Transfected A549 and H1975 cells were transferred in 96-well plates at a density of 5×10^3 cells/well. Every transfection group was repeated in six wells. The transfected cells were incubated in normal cell culture condition for 24, 48 and 72 hours. For IC50 analysis, after transfection for 48 hours, A549 and H1975 cells were exposed to 2.5, 5, 10, 20, 40, and 80 μM of DDP (Sigma-Aldrich, St. Louis, MO, USA) for another 24 hours. At indicated times, 10 μL of CCK-8 solution (Dojindo, Tokyo, Japan) was added in each well. With another 2 hours incubation in the dark, the optical density value at 450 nm (OD 450 nm value) was measured with a microplate reader (Bio-Rad, Hercules,

CA, USA). With OD450 values, DDP-induced inhibition rate (%) of cell viability was calculated.

Transwell assays for cell migration and invasion

After 48 hours transfection, A549 and H1975 cells were collected, and 5×10^5 cells were resuspended in 200 μL of serum-free RPMI 1640. For migration assay, transwell chamber (Costar, Shanghai, China) was placed in a 24-well plate, and cell suspension was loaded in the upper chamber. The lower chamber was filled with 400 μL of RPMI 1640 containing 20% FBS (Hyclone). The transwell system was incubated in normal cell culture condition for another 48 hours. For invasion assay, the chamber was precoated with Matrigel (BD Biosciences, Mountain View, CA, USA) membrane by incubating with Matrigel: RPMI 160 (1: 9) at room temperature for overnight. Then, the migrated cells or invaded cells on the lower surface were fixed with 4% paraformaldehyde for 15 minutes, and dyed with 0.25% crystal violet for 20 minutes at room temperature. Finally, the migratory and invasive cells were observed under microscope, and five randomly selected fields were captured at magnification of 100×.

Western blotting

Total protein in tissues and cell lines was extracted in RIPA reagent (Beyotime, Shanghai, China) supplemented with protease inhibitor PMSF (Sigma-Aldrich). Then, an aliquot of protein sample (20 μg) was separated by sodium dodecyl sulfate-polyacrylamide gel electrophoresis, and then transferred onto polyvinylidene fluoride (PVDF; Millipore) membrane. After blocking in 5% skin milk, the membranes were incubated in primary antibodies from Proteintech (Deansgate, Manchester, UK) including anti-HMGB1 (10829-1-AP, 1: 2000), antiproliferating cell nuclear antigen (PCNA; 10 205-2-AP, 1: 10000), anti-E-cadherin (E-cad; 20 874-1-AP, 1: 50000), anti-N-cadherin (N-cad; 22 018-1-AP, 1: 10000), and anti-GAPDH (10494-1-AP, 1: 40000) at 4°C for overnight, and in secondary antibody anti-rabbit IgG-HRP (sc-2357, 1: 5000) from Santa Cruz (Shanghai, China) at room temperature for 2 hours. The protein blots were developed using ECL reagent (Millipore), and captured by Chemiluminescence (Thermo Fisher Scientific). GAPDH was the internal control.

Flow cytometry (FCM) for apoptosis rate and caspase-3 activity

After transfection for 48 hours, A549 and H1975 cells in six-well plate were exposed to 5 μM of DDP (Sigma-Aldrich) for another 24 hours. Cell apoptosis was

measured by FCM using Annexin V fluorescein isothiocyanate (FITC) apoptosis detection kit (Beyotime) and CaspGLOW fluorescein active caspase-3 staining kit (Thermo Fisher Scientific) following the manufacturer's instructions. Apoptosis rate (%) was measured using a FACScan flow cytometer (BD Biosciences) equipped with CellQuest software (BD Biosciences). Caspase-3 fluorescence intensity was analyzed by FCM, and relative caspase-3 activity was calculated comparing to control cells.

Dual-luciferase reporter assay

The full length of circ_0007385 and 3'-untranslated region of HMGB1 (HMGB1 3'UTR) were inserted into pGL4 luciferase reporter vector (Promega, Fitchburg, WI, USA), thus establishing the wild-type of circ_0007385 vectors (circ_0007385 WT) and HMGB1 3'UTR vectors (HMGB1 3'UTR WT). Then, the putative binding sites of miR-519d-3p in circ_0007385 and HMGB1 3'UTR were mutated, and their mutated-type (MUT) vectors (circ_0007385 MUT and HMGB1 3'UTR MUT) were similarly constructed. A549 and H1975 cells were passaged in a 24-well plate at a density of 5×10^4 cells/well, and cotransfected with miR-519d-3p/NC mimic (10 μM) and either circ_0007385 WT/MUT (300 ng) or HMGB1 3'UTR WT/MUT (300 ng) using Lipofectamine 3000 reagent (Invitrogen) according to the manufacturer's instruction. Post transfection for 48 hours, the Firefly and Renilla luciferase activities were measured on dual luciferase reporter (DLR) system (Promega). Relative luciferase activity was the ratio of Firefly/Renilla luciferase activity, normalized to control cells.

Xenograft experiment

A total of 10 BALB/c nude mice (5–7-week-old, male) were purchased from Vital River Laboratory Animal Technology (Beijing, China). The mice were divided into sh-circ group ($n = 5$) and sh-NC group ($n = 5$), and then were subcutaneously injected with A549 cells (5×10^6 cells) transfected with sh-circ or sh-NC into the right flanks. The xenograft mice were further raised for days, and the dimension of neoplasms was measured every seven days after transplantation. The tumor volume (mm^3) was calculated using the formula: (length×width^2)/2. The tumor weight (mg) was measured on electronic balance on the day 28 after euthanasia of mice. This animal experiment was approved by the Ethics Committee of the Gansu Wuwei Tumor Hospital, and all procedures were strictly conformed to the Guide for the Care and Use of Laboratory Animals from NIH.

Statistical analysis

All data were analyzed using GraphPad software 7.0 (GraphPad, San Diego, CA, USA). The P-values were obtained using Student's t-test, one-way analysis of variance, and Pearson correlation coefficient test. $P < 0.001$ was considered statistically significant, and labeled using **.

Results

### Circ_0007385 was upregulated in NSCLC tumor tissues and cells

A group of 75 primary NSCLC tumor tissues were collected, as well as the paired adjacent normal tissues. The expression of circ_0007385 in tissues was detected using RT-qPCR, and circ_0007385 level was higher in NSCLC tumors (Fig 1a), and was even higher in advanced tumors (III + IV stages; n = 43) (Fig 1b). Moreover, the five-year overall survival of these NSCLC patients was about 18% in the circ_0007385 high expression group (≥mean, $n = 39$; Fig 1c), and about 39% in the circ_0007385 low expression group (<mean, $n = 36$; Fig 1c). Expression of circ_0007385 in human NSCLC cell lines was also detected, and RT-qPCR data showed an overall upregulation of circ_0007385 in A549, HCC827, H1975, and H2342 cells versus 16HBE (Fig 1d). These results indicated that circ_0007385 was deregulated in NSCLC tissues and cells, suggesting a potential biological role of circ_0007385 in malignant progression of NSCLC cells.

Interfering circ_0007385 depressed NSCLC cell proliferation, migration and invasion in vitro

The expression of circ_0007385 was exogenously silenced using shRNA transfection, and RT-qPCR analysis confirmed transfection efficiency. As shown in Fig 2a, circ_0007385 level was significantly lowered in A549 and H1975 cells with sh-circ transfection. Then, the role of circ_0007385 silence was further investigated in A549 and H1975 cells. CCK-8 assay displayed a decrease of cell viability in circ_0007385-downregulated cells, compared to sh-NC-transfected cells (Fig 2b and c). Transwell assays measured that migratory cells and invasive cells were declined by sh-circ introduction (Fig 2d and e). In addition, western blotting result showed an increase of E-cad, and a decrease of PCNA and N-cad in response to sh-circ transfection in A549 and H1975 cells (Fig 2f). These data together demonstrated that circ_0007385 knockdown could depress cell proliferation, migration and invasion in NSCLC cells in vitro.

Silencing circ_0007385 inhibited DDP resistance of NSCLC cells in vitro

Next, the role of circ_0007385 in DDP resistance of NSCLC cells was explored. With treatment of 2.5, 5, 10,
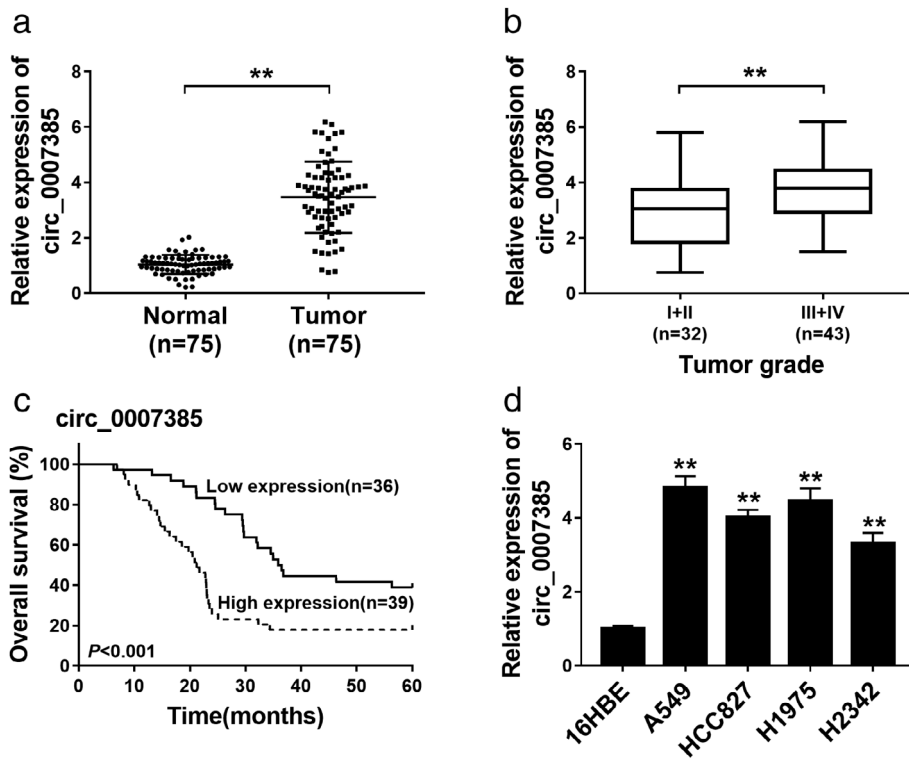
Figure 1 The expression of hsa_circ_0007385 (circ_0007385) in non-small cell lung cancer (NSCLC) tissues and cells. (**a** and **b**) RT-qPCR measured relative expression of circ_0007385 in (**a**) NSCLC tumor tissues (Tumor, $n = 75$) and adjacent normal tissues (Normal, $n = 75$) and (**b**) low grade (I + II; $n = 32$) and high grade (III + IV; $n = 43$) of tumors. (**c**) Kaplan-Meier survival curve showed the overall survival (%) of NSCLC patients with circ_0007385 high expression (≥mean, $n = 39$) or low expression (<mean, $n = 36$). (**d**) RT-qPCR measured circ_0007385 expression level in human NSCLC cell lines (A549, HCC827, H1975, and H2342), and one human bronchial epithelial cell line (16HBE). **$P < 0.01$.

20, 40, and 80 μM of DDP, cell viability inhibition was observed in transfected A549 and H1975 cells; moreover, IC50 of DDP was reduced by sh-circ transfection from 10.39 to 5.92 μM in A549 cells, and from 13.69 to 7.77 μM in H1975 cells (Fig 3a and b). Moreover, circ_0007385 deletion enhanced apoptosis rate (Fig 3c and d) and caspase-3 activity (Fig 3e and f) in A549 and H1975 cells with 5 μM of DDP treatment. These data suggested a suppression of circ_0007385 knockdown on DDP resistance in NSCLC cells in vitro.

## Circ_0007385 negatively regulated miR-519d-3p via target binding

By searching the StarBase database, we took miR-519d-3p as a candidate for circ_0007385, and the potential binding site between the circ_0007385 WT and miR-519d-3p is shown in Fig 4a. Exogenous transfection of miR-519d-3p mimic obviously attenuated luciferase activity of pGL4 report vector carrying circ_0007385 WT in A549 and H1975 cells (Fig 4b and c). Additionally, we confirmed a downregulation of miR-519d-3p in NSCLC tumor tissues ($n = 75$; Fig 4d), and its expression was negatively correlated with circ_0007385 ($r = 0.6273$, $P < 0.001$; Fig 4e). In addition, expression of miR-519d-3p was lower in A549 and H1975 cells than that in 16HBE cells (Fig 4f), and was upregulated in A549 and H1975 cells with circ_0007385 knockdown (Fig 4g). These

results suggested that circ_0007385 could serve as a ceRNA for miR-519d-3p via target binding in NSCLC.

Deletion of miR-519d-3p overturned the suppressive effect of circ_0007385 on NSCLC cell proliferation, migration, invasion, and DDP resistance in vitro

Thereby, we speculated that circ_0007385 modulate the malignant progression of NSCLC cells by directly regulating miR-519d-3p expression. The anti-miR-519d-3p was used to delete miR-519d-3p expression in A549 and H1975 cells, and RT-qPCR further validated this silencing efficiency (Fig 5a). Cell proliferation was inhibited by circ_0007385 downregulation in A549 and H1975 cells, which was abolished by the presence of anti-miR-519d-3p, as described by improved cell viability (Fig 5b and c) and PCNA expression (Fig 5f). Cell migration and invasion were also restrained by circ_0007385 silencing, and then rescued by anti-miR-519d-3p transfection, as evidenced by higher numbers of transwell migratory and invasive cells (Fig 5d and e), increased N-cad expression, and decreased E-cad level (Fig 5f). On the contrary, the promotion of circ_0007385 knockdown on DDP sensitivity was abrogated by the deletion of miR-519d-3p, as depicted by elevated IC50 (Fig 5g), and descended apoptosis rate (Fig 5h) and caspase-3 activity (Fig 5i and j). Collectively, these outcomes showed that miR-519d-3p inhibition
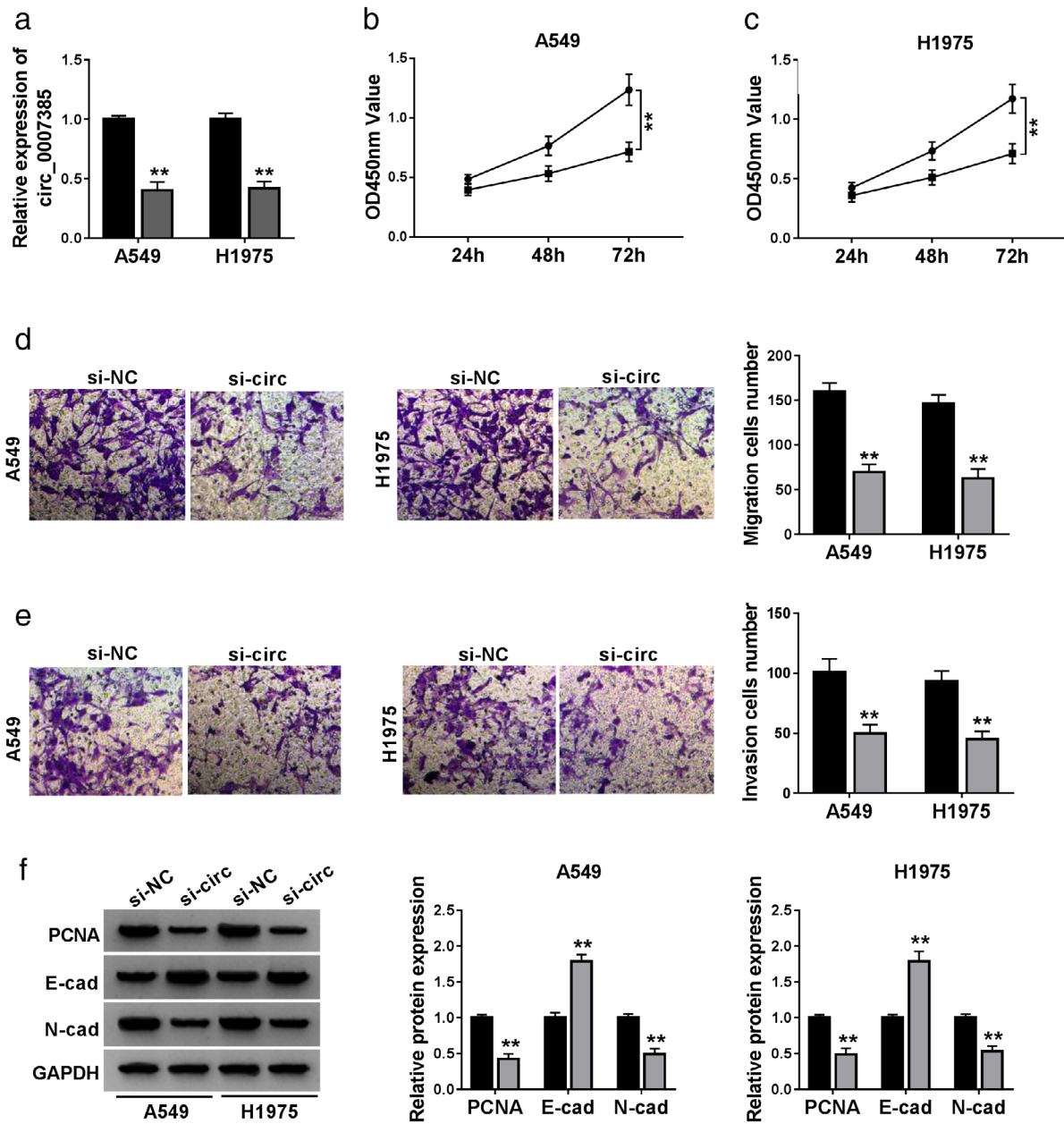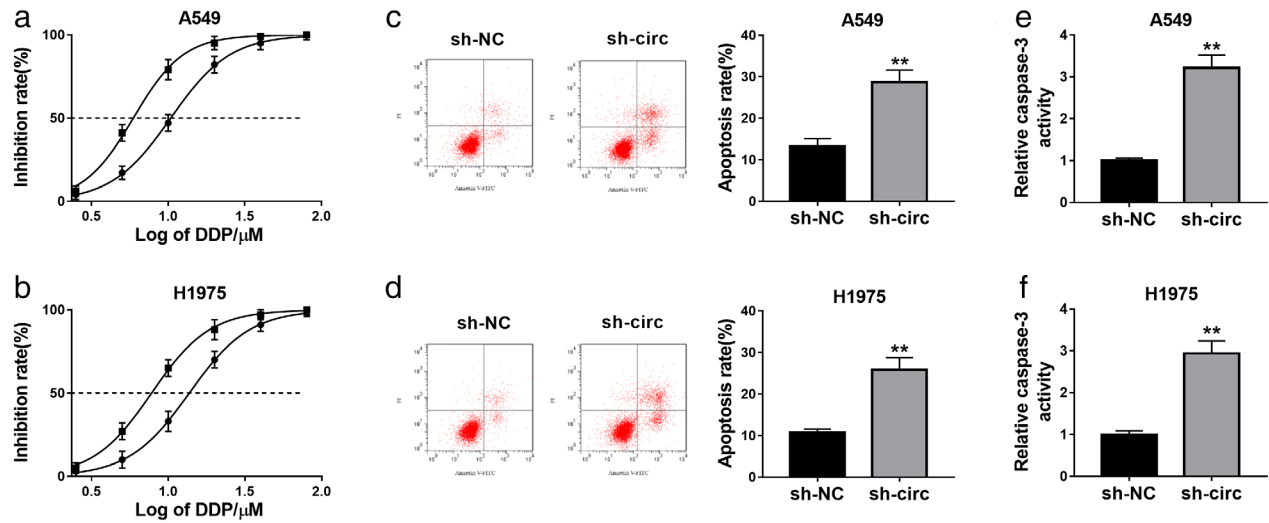
Figure 2 The effect of circ_0007385 knockdown on NSCLC cell proliferation, migration and invasion in vitro. (**a–f**) A549 and H1975 cells were transfected with shRNA targeting circ_0007385 (sh-circ) or the negative control sh-NC for 48 hours. (**a**) RT-qPCR confirmed the circ_0007385 level () sh-NC, () sh-circ. (**b** and **c**) CCK-8 assessed optical density value at 450 nm (OD450 nm value) at 24, 48 and 72 hours () sh-NC, () sh-circ; (—●—) sh-NC, (—■—) sh-circ. (**d** and **e**) Transwell assays determined the number of migratory and invasive cells () sh-NC, () sh-circ; (■) sh-NC, (▨) sh-circ. (**f**) Western blotting detected protein expression of the proliferating cell nuclear antigen (PCNA), E-cadherin (E-cad) and N-cadherin (N-cad) (■) sh-NC, (▨) sh-circ; (■) sh-NC, (▨) sh-circ. **$P < 0.01$.

could overturn the suppressive effect of circ_0007385 knockdown on cell proliferation, migration, invasion, and DDP resistance in A549 and H1975 cells, suggesting the role of circ_0007385 in the malignant progression of NSCLC cells by sponging miR-519d-3p.

HMGB1 was a target gene of miR-519d-3p in NSCLC cells

To investigate the downstream functional gene of miR-519d-3p, we employed the StarBase database to predict

Figure 3 The effect of circ_0007385 knockdown on cisplatin (DDP) sensitivity of NSCLC cells in vitro. (**a–f**) A549 and H1975 cells were transfected with sh-circ or sh-NC, and then treated with DDP for 48 hours. (**a** and **b**) CCK-8 measured the inhibition rate (%) of cell viability after treatment of 0, 2.5, 5, 10, 20, 40, and 80 μM of DDP (━●━) sh-NC IC50 = 10.39, (━■━) sh-circ IC50 = 5.92; (━●━) sh-NC IC50 = 13.69, (━■━) sh-circ IC50 = 7.77. IC50, half maximal inhibitory concentration. (**c** and **d**) Flow cytometry (FCM) and Annexin V fluorescein isothiocyanate (FITC) apoptosis detection kit examined apoptosis rate (%) after treatment of 10 μM of DDP. (**e** and **f**) FCM and fluorescein active caspase-3 staining kit examined relative caspase-3 activity after treatment of 10 μM of DDP. ****P* < 0.01.
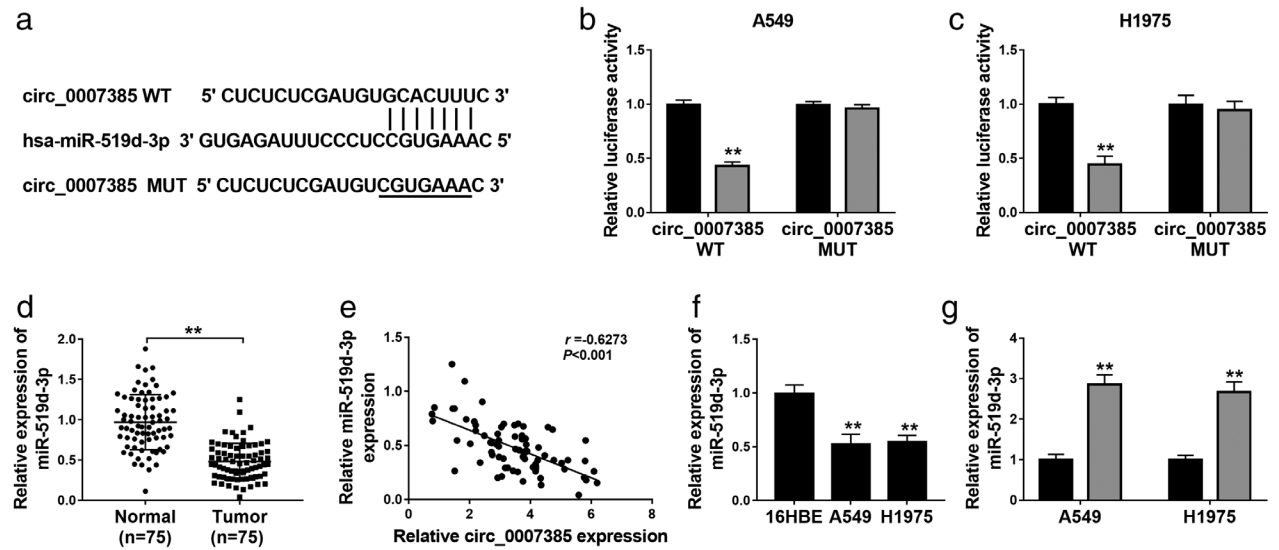
Figure 4 The target relationship between circ_0007385 and miRNA (miR)-519d-3p. (**a**) The StarBase algorithms showed the complementary binding sequence of miR-519d-3p on the wild-type of circ_0007385 (circ_0007385 WT). The mutant type of circ_0007385 (circ_0007385 MUT) was constructed. (**b** and **c**) Dual-luciferase reporter assay evaluated relative luciferase activity of circ_0007385 WT/MUT in A549 and H1975 cells transfected with miR-519d-3p mimic (miR-519d-3p) or miR-NC mimic (miR-NC) (■) miR-NC, (▨) miR-519d-3p; () miR-NC, () miR-519d-3p. (**d**) RT-qPCR detected relative expression of miR-519d-3p in tissues in the Normal (*n* = 75) and Tumor (*n* = 75) groups. (e) Pearson correlation coefficient (*r*) analysis determined the correlation between circ_0007385 and miR-519d-3p expression in NSCLC tumors (*n* = 75). (**f** and **g**) RT-qPCR detected miR-519d-3p level in (**f**) 16HBE, A549 and H1975 cells, and (**g**) A549 and H1975 cells transfected with sh-circ or sh-NC (■) sh-NC, (▨) sh-circ. ****P* < 0.01.
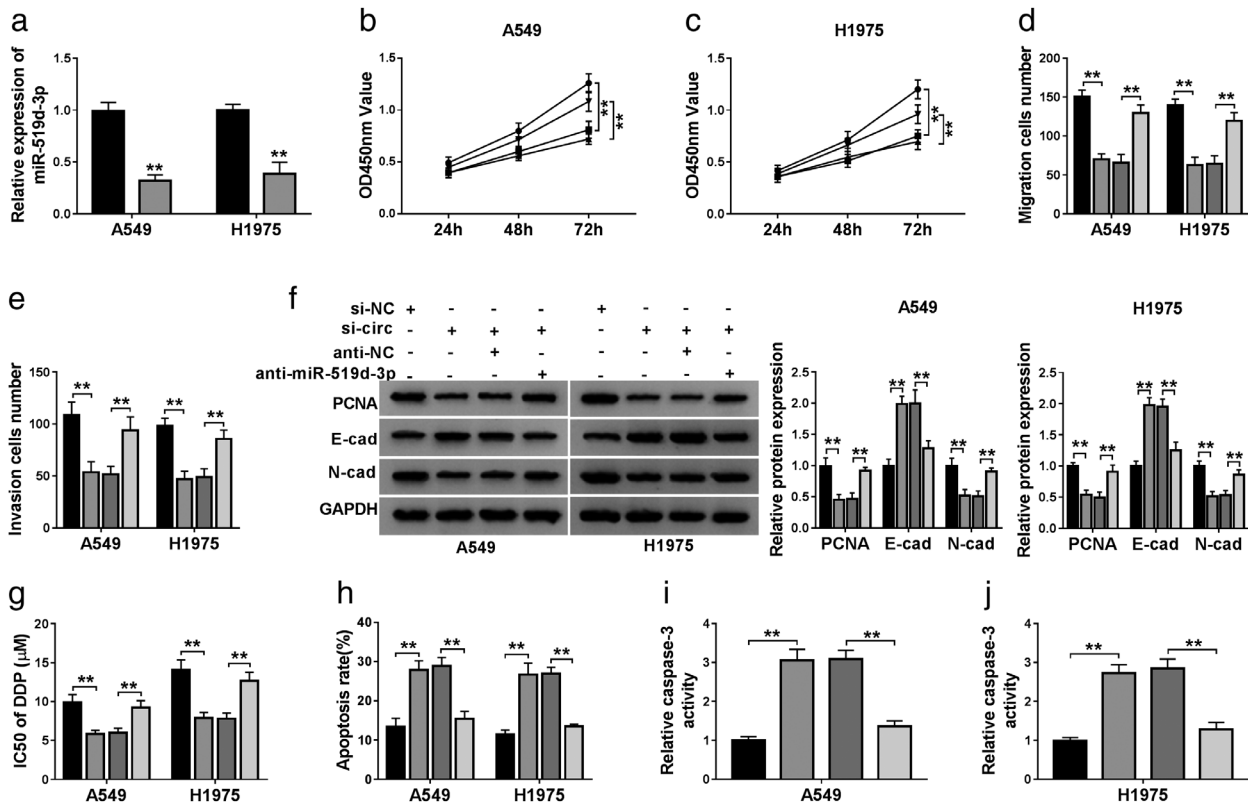
Figure 5 The contribution of miR-519d-3p to the effect of circ_0007385 knockdown in NSCLC cells in vitro. (**a**) RT-qPCR measured miR-519d-3p level in A549 and H1975 cells transfected with miR-519d-3p inhibitor (anti-miR-519d-3p) or its control miR-NC inhibitor (anti-NC) (■) anti-NC, (□) anti-miR-519d-3p. (**b–j**) A549 and H1975 cells were transfected with sh-circ or sh-NC, and cotransfected with sh-circ and anti-miR-519d-3p, or sh-circ and anti-NC. (**b** and **c**) CCK-8 assessed OD450 nm value on 24, 48 and 72 hours (—●—) sh-NC, (—■—) sh-circ, (—▲—) sh-circ+anti-NC, (—▼—) sh-circ+anti-miR-519d-3p; (—●—) sh-NC, (—■—) sh-circ, (—▲—) sh-circ+anti-NC, (—▼—) sh-circ+anti-miR-519d-3p. (**d** and **e**) Transwell assays determined the numbers of migratory and invasive cells (■) sh-NC, (□) sh-circ, (□) sh-circ+anti-NC, (□) sh-circ+anti-miR-519d-3p; (■) sh-NC, (□) sh-circ, (□) sh-circ+anti-NC, (□) sh-circ+anti-miR-519d-3p. (**f**) Western blotting detected protein expression of the PCNA, E-cad and N-cad (■) sh-NC, (□) sh-circ, (□) sh-circ+anti-NC, (□) sh-circ+anti-miR-519d-3p; (■) sh-NC, (□) sh-circ, (□) sh-circ+anti-NC, (□) sh-circ+anti-miR-519d-3p. (**g–j**) A549 and H1975 cells transfected with sh-circ or sh-NC were treated with DDP for 48 hours. (**g**) CCK-8 measured IC50 of DDP after treatment of 0, 2.5, 5, 10, 20, 40, and 80 μM of DDP (■) sh-NC, (□) sh-circ, (□) sh-circ+anti-NC, (□) sh-circ+anti-miR-519d-3p. (**h**) FCM examined apoptosis rate (%) (■) sh-NC, (□) sh-circ, (□) sh-circ+anti-NC, (□) sh-circ+anti-miR-519d-3p and (**i** and **j**) caspase-3 activity after treatment of 10 μM of DDP (■) sh-NC, (□) sh-circ, (□) sh-circ+anti-NC, (□) sh-circ+anti-miR-519d-3p; (■) sh-NC, (□) sh-circ, (□) sh-circ+anti-NC, (□) sh-circ+anti-miR-519d-3p. **$*P < 0.01$.

the binding site between miR-519d-3p and HMGB1 (Fig 6a). Dual-luciferase reporter assay determined a significant loss of luciferase activity of HMGB1 3'UTR WT in A549 and H1975 cells transfected with miR-519d-3p mimic (Fig 6b and c). In NSCLC, expression of HMGB1 protein was upregulated in three tumor tissues (Fig 6d) and two cell lines (Fig 6e), paralleled with that in paired normal tissues and 16HBE cells, respectively. As showed, miR-519d-3p mimic transfection downregulated, whereas anti-miR-519d-3p transfection upregulated HMGB1 expression in A549 and H1975 cells (Fig 6g and h). Incidentally, the transfection efficiency was determined by RT-qPCR (Figs 5a and 6f). Furthermore, sh-circ transfection caused inhibition on HMGB1 expression, which was

attenuated by miR-519d-3p deletion (Fig 6i and j). These data suggested that circ_0007385 could affect HMGB1 via sponging miR-519d-3p in NSCLC cells. Thus, we wondered the influence of HMGB1 restoration on the suppressive role of circ_0007385 knockdown in NSCLC cell malignancy. The HMGB1 restoration was mediated by overexpression vector transfection in A549 and H1975 cells (Fig 7a), and then blocked the inhibition of circ_0007385 knockdown on cell viability (Fig 7b and c), transwell migration and invasion (Fig 7d and e), PCNA and N-cad expression (Fig 7f), as well as abrogated E-cad expression promotion (Fig 7f). In addition, the suppression of circ_0007385 knockdown on DDP resistance was also
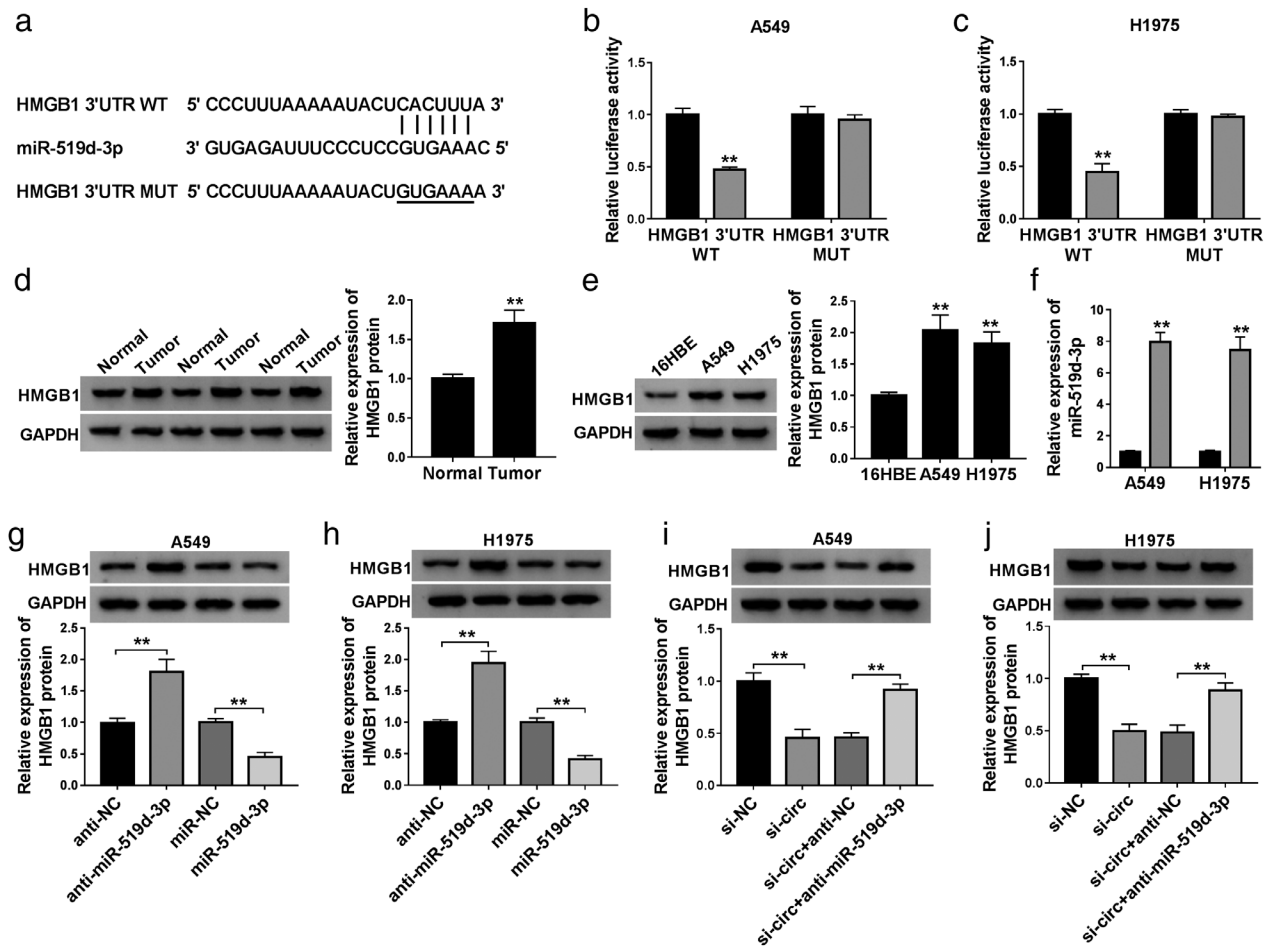
Figure 6 The target relationship between miR-519d-3p and HMGB1. (**a**) The StarBase algorithms showed the complementary binding sequence of miR-519d-3p on the wild-type of HMGB1 3′UTR (HMGB1 3′UTR WT). The mutant type of HMGB1 3′UTR (HMGB1 3′UTR MUT) was constructed. 3′UTR, 3′ untranslated region. (**b** and **c**) Dual-luciferase reporter assay evaluated relative luciferase activity of HMGB1 3′UTR WT/MUT in A549 and H1975 cells transfected with miR-519d-3p or miR-NC (■) miR-NC, (▨) miR-519d-3p; () miR-NC, ()miR-519d-3p. (**d** and **e**) Western blotting confirmed the expression of HMGB1 protein in (**d**) three paired tissues (Normal and Tumor groups), and (**e**) 16HBE, A549 and H1975 cells. (**f**) RT-qPCR detected miR-519d-3p expression in A549 and H1975 cells transfected with miR-519d-3p or miR-NC (■) miR-NC, (▨) miR-519d-3p. (**g** and **h**) Western blotting examined HMGB1 protein expression in A549 and H1975 cells transfected with anti-NC, anti-miR-519d-3p, miR-NC, or miR-519d-3p. (**i** and **j**) Western blotting examined HMGB1 protein expression in A549 and H1975 cells transfected with sh-NC or sh-circ, and cotransfected with sh-circ and anti-NC or anti-miR-519d-3p. **$P < 0.01$.

counteracted with the administration of HMGB1 over-expression vector, as manifested by recovered IC50 (Fig 7g), and declined apoptosis rate (Fig 7h) and caspase-3 activity (Fig 7i and j). These results suggested that circ_0007385 silencing suppressed malignant behaviors and DDP resistance of NSCLC cells in vitro by downregulating HMGB1 via miR-519d-3p.

Silenced circ_0007385 retarded the tumor growth of NSCLC cells in vivo

To explore the impact of circ_0007385/miR-519d-3p/HMGB1 axis on the tumorigenesis of NSCLC cells in vivo,

A549 cells were transfected with sh-circ or sh-NC, and then subcutaneously injected into the right flanks of nude mice ($n = 5$). Tumor growth of A549 cells in mice was dramatically retarded in the sh-circ group compared with the sh-NC group, as indicated by decreased tumor volume (Fig 8a) and tumor weight (Fig 8b). Molecularly, sh-circ transfection led to circ_0007385 knockdown in the tissues from neoplasm (Fig 8c), accompanied with miR-519d-3p upregulation (Fig 8d) and HMGB1 protein downregulation (Fig 8e). These data demonstrated that circ_0007385 knockdown retarded tumor growth of NSCLC cells in vivo partially through synergistically regulating miR-519d-3p and HMGB1.
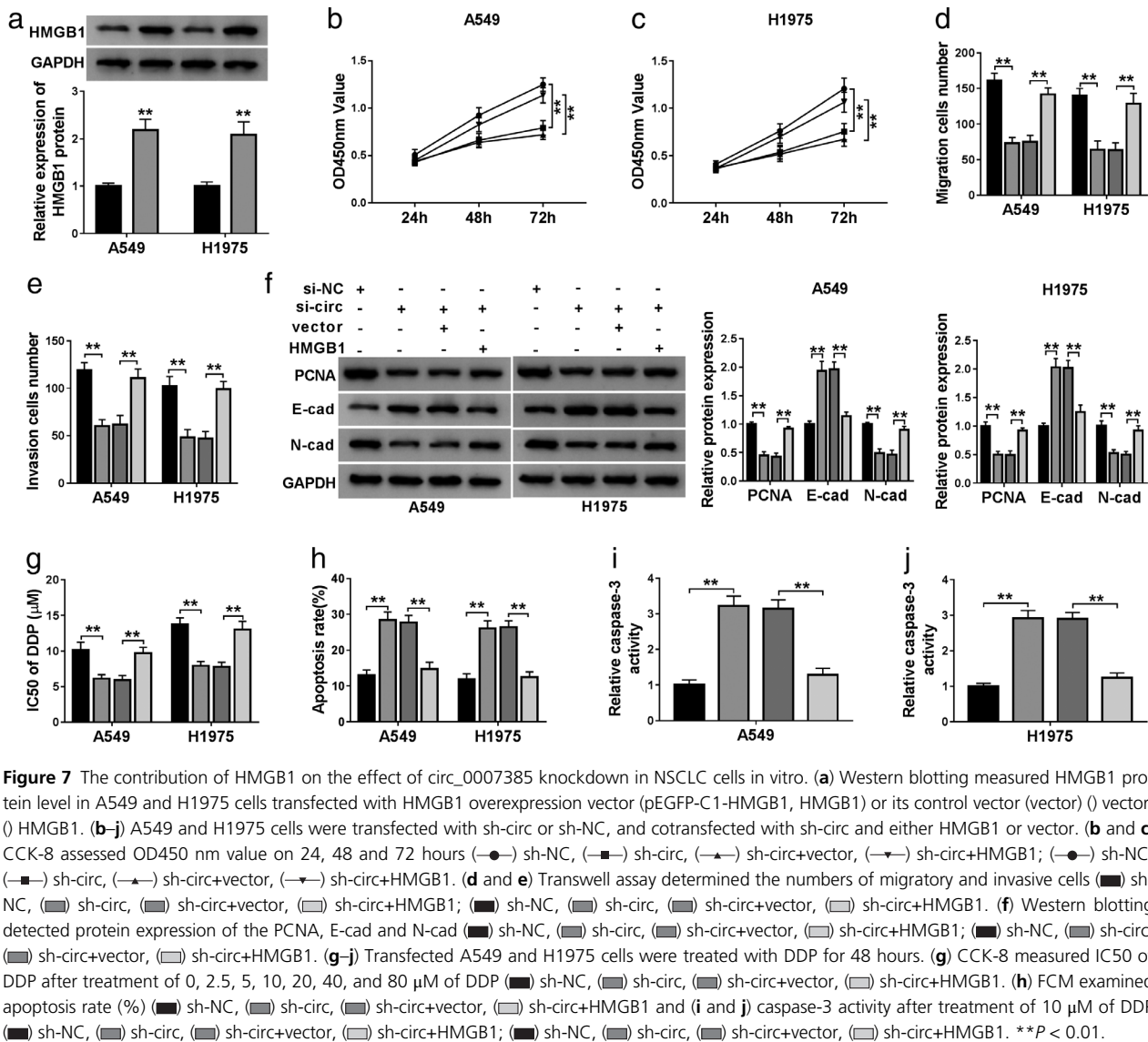
Figure 7 The contribution of HMGB1 on the effect of circ_0007385 knockdown in NSCLC cells in vitro. (**a**) Western blotting measured HMGB1 protein level in A549 and H1975 cells transfected with HMGB1 overexpression vector (pEGFP-C1-HMGB1, HMGB1) or its control vector (vector) () vector, () HMGB1. (**b**–**j**) A549 and H1975 cells were transfected with sh-circ or sh-NC, and cotransfected with sh-circ and either HMGB1 or vector. (**b** and **c**) CCK-8 assessed OD450 nm value on 24, 48 and 72 hours (—●—) sh-NC, (—■—) sh-circ, (—▲—) sh-circ+vector, (—▼—) sh-circ+HMGB1; (—●—) sh-NC, (—■—) sh-circ, (—▲—) sh-circ+vector, (—▼—) sh-circ+HMGB1. (**d** and **e**) Transwell assay determined the numbers of migratory and invasive cells (■) sh-NC, (▨) sh-circ, (▨) sh-circ+vector, (☐) sh-circ+HMGB1; (■) sh-NC, (▨) sh-circ, (▨) sh-circ+vector, (☐) sh-circ+HMGB1. (**f**) Western blotting detected protein expression of the PCNA, E-cad and N-cad (■) sh-NC, (▨) sh-circ, (▨) sh-circ+vector, (☐) sh-circ+HMGB1; (■) sh-NC, (▨) sh-circ, (▨) sh-circ+vector, (☐) sh-circ+HMGB1. (**g**–**j**) Transfected A549 and H1975 cells were treated with DDP for 48 hours. (**g**) CCK-8 measured IC50 of DDP after treatment of 0, 2.5, 5, 10, 20, 40, and 80 μM of DDP (■) sh-NC, (▨) sh-circ, (▨) sh-circ+vector, (☐) sh-circ+HMGB1. (**h**) FCM examined apoptosis rate (%) (■) sh-NC, (▨) sh-circ, (▨) sh-circ+vector, (☐) sh-circ+HMGB1 and (**i** and **j**) caspase-3 activity after treatment of 10 μM of DDP (■) sh-NC, (▨) sh-circ, (▨) sh-circ+vector, (☐) sh-circ+HMGB1; (■) sh-NC, (▨) sh-circ, (▨) sh-circ+vector, (☐) sh-circ+HMGB1. **$P < 0.01$.

Discussion

circRNAs have been found to be differentially expressed in NSCLC patients. For example, the expression profile of circRNAs in peripheral whole blood of patients ($n = 5$) with lung adenocarcinoma (LUAD, a main subtype of NSCLC) has been identified.[24] Therefore, circRNAs in blood have already been considered as potent biomarkers for the prognosis and therapeutic response of NSCLC.[25] CircRNAs microarray analysis has identified many differently expressed circRNAs in NSCLC tumor tissues ($n = 3$) paralleled with matched nontumor tissues.[19, 26] Moreover, RNA sequencing analyses profiled circRNA expression patterns in 10 pairs of LUAD and lung squamous cell carcinoma (LUSC), two subtypes of NSCLC, and two circRNAs

(hsa_circ_0001073 and hsa_circ_0001495) have been proposed to distinguish LUAD and LUSC.[27] Functionally, multiple oncogenic circRNAs, such as circRNA ARHGAP10, circNT5E, and circ-ZKSCAN1, have been certified to contribute to NSCLC cell proliferation and metastasis in vitro and in vivo;[26, 28, 29] DDP resistance in NSCLC cells has also been declared to be affected by several circRNAs, including circ-SMARCA5, circ_0076305 and circ_0001946.[30-32]

According to the findings of Jiang *et al.*,[19] circ_0007385 might function as an oncogene in NSCLC carcinogenesis, and miR-181 was a target of circ_0007385. Here, we reported the upregulation of circ_0007385 in NSCLC tissues and cell lines, and discovered a suppressive effect of circ_0007385 deletion on cell proliferation, migration and
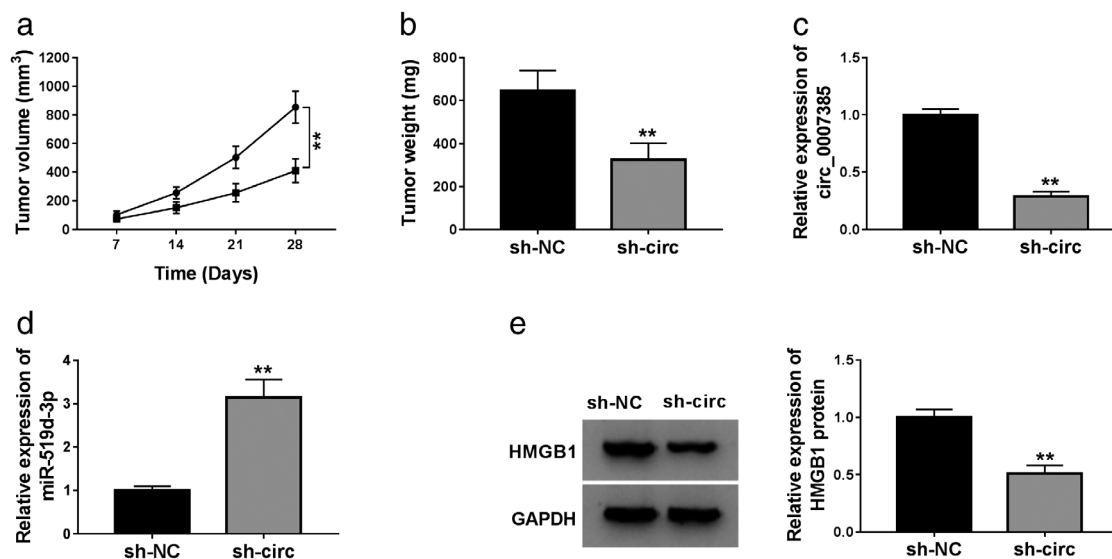
Figure 8 The effect of circ_0007385 knockdown on tumor growth in vivo. A549 cells were transfected with sh-circ or sh-NC, and then subcutaneously injected into the right flanks of nude mice (*n* = 5). (**a**) Tumor volume was measured every seven days after cell transplantation (—●—) sh-NC, (—■—) sh-circ. (**b**) Tumor weight was examined on day 28. (**c** and **d**) RT-qPCR detected circ_0007385 and miR-519d-3p expression levels in tissues from neoplasm. (**e**) Western blotting evaluated HMGB1 protein expression level in tissues from neoplasm.

invasion in A549 and H1975 cells, and tumor growth in vivo. These findings were in accordance with a previous study in A549 and H1299 cells.[19] Similarly, we predicted and confirmed miR-519d-3p as a novel target of circ_0007385; notably, HMGB1 as a downstream functional gene of circ_0007385/miR-519d-3p axis was further validated. Furthermore, we noticed that circ_0007385 knockdown suppressed DDP resistance of NSCLC cells in vitro, as evidenced by the lowered IC50 of DDP, and elevated DDP-induced apoptosis rate and caspase-3 activity in A549 and H1975 cells. Clinically, we discovered that low expression of circ_0007385 might predict a relative better overall survival in NSCLC patients, hinting a potential biomarker of circ_0007385 for the prognosis of NSCLC tumors. Therefore, we established a circ_0007385/miR-519d-3p/HMGB1 pathway underlying the oncogenic role of circ_0007385 in NSCLC.

Emerging evidences on the tumor suppressive role of miR-519d-3p have been reported in cell progression in different cancers, such as colorectal cancer, oral squamous cell carcinoma, and pancreatic cancer.[33–35] Unfortunately, there has been little research on its role in lung cancer cells to date, except for the association with immune infiltration, cell proliferation and invasion in LUAD.[36, 37] Nevertheless, miR-519d-3p expression has been reported to have no significant correlation to clinical characteristics (age, gender, smoking history, and tumor staging).[17] Herewith, we confirmed the downregulation of miR-519d-3p in NSCLC tissues and cells, which is consistent with other publications.[18, 36, 37] In

addition, miR-519d-3p expression has been found to be correlated to circ_0007385, and downregulation of miR-519d-3p could reverse circ_0007385 silence-mediated inhibition on cell proliferation, migration, invasion, and DDP resistance in A549 and H1975 cells. Incidentally, miR-519d-3p had previously demonstrated as inhibitory factor of DDP resistance in colorectal, breast and ovarian cancers.[38–40] Taking these findings together, we concluded that there is a close association among miR-519d-3p, tumor cell progression and DDP resistance in cancers. More importantly, we validated circ_0007385 as a novel ceRNA for miR-519d-3p, and HMGB1 as a new downstream target of miR-519d-3p.

HMGB1 had been assessed as one diagnostic and prognostic biomarker in NSCLC, especially in LUAD.[41] Expression of HMGB1 has been reported to be highly expressed in NSCLC tissues, sera and pleural effusions from NSCLC patients.[42, 43] Here, we observed upregulation of HMGB1 in three NSCLC tissues and two cell lines (A549 and H1975). Functionally and mechanically, HMGB1 has been previously described to be a downstream target of miRNAs in NSCLC cell proliferation, migration and invasion, such as miR-520a-3p, miR-449a and miR-200c.[44-46] Here, we clarified a pro-proliferation effect of HMGB1 in A549 and H1975 cells with circ_0007385 knockdown. Molecularly, HMGB1 was targeted by miR-519d-3p, and circ_0007385 could regulate HMGB1 expression by sponging miR-519d-3p. On the other hand, HMGB1 could sensitize NSCLC cells to chemotherapeutic drugs including DDP.[47] Interfering HMGB1 increased DDP sensitivity in A549/DDP cells

by inducing apoptosis, and inhibiting cell viability and autophagy;[47, 48] on the contrary, restoring HMGB1 reduced DDP sensitivity by facilitating cell proliferation, migration and invasion in A549 and H1299 cells via SNHG14/miR-34a/HMGB1 axis.[49] Here, we determined that HMGB1 upregulation could contribute to DDP resistance in circ_0007385-silenced A549 and H1975 cells, as evidenced by an increase in cell viability and decrease of DDP-induced apoptosis rate and caspase-3 activity.

However, the contribution of circ_0007385/miR-519d-3p/HMGB1 to many other important cell behaviors such as cell-cycle regulation, epithelial-mesenchymal transition and autophagy has not been discussed in our study. .[12, 48] However, this study may have provided first-hand evidence on the role of circ_0007385 in DDP resistance in NSCLC cells, and suggested a novel circ_0007385/miR-519d-3p/HMGB1 regulatory pathway in the malignant development of NSCLC.

In conclusion, this study demonstrated that circ_0007385 was upregulated in NSCLC tissues and cells, and its high expression could predict a shorter five-year overall survival. The silencing of circ_0007385 could suppress cell proliferation, migration, invasion, and DDP resistance in NSCLC cells in vitro through regulating miR-519d-3p/HMGB1 axis, accompanied with tumor growth inhibition in vivo. These outcomes might enhance our understanding of molecular mechanisms underlying the malignant progression of NSCLC.

Disclosure

References

1 Bray F, Ferlay J, Soerjomataram I, Siegel RL, Torre LA, Jemal A. Global cancer statistics 2018: GLOBOCAN estimates of incidence and mortality worldwide for 36 cancers in 185 countries. *CA Cancer J Clin* 2018; **68**: 394–424.

2 Molina JR, Yang P, Cassivi SD, Schild SE, Adjei AA. Non-small cell lung cancer: Epidemiology, risk factors, treatment, and survivorship. *Mayo Clin Proc* 2008; **83**: 584–94.

3 Wang C, Jiang Y, Lei Q *et al.* Potential diagnostic and prognostic biomarkers of circular RNAs for lung cancer in China. *Biomed Res Int* 2019; **2019**: 8023541.

4 Mason J, Blyth B, MacManus MP *et al.* Treatment for non-small-cell lung cancer and circulating tumor cells. *Lung Cancer Manag* 2017; **6**: 129–39.

5 Ettinger DS, Wood DE, Aisner DL *et al.* Non-small cell lung cancer, version 5.2017, NCCN clinical practice guidelines in oncology. *J Natl Compr Canc Netw* 2017; **15**: 504–35.

6 Kris MG, Gaspar LE, Chaft JE *et al.* Adjuvant systemic therapy and adjuvant radiation therapy for stage I to IIIA completely resected non-small-cell lung cancers: American Society of Clinical Oncology/Cancer Care Ontario clinical practice guideline update. *J Clin Oncol* 2017; **35**: 2960–74.

7 Ghosh S. Cisplatin: The first metal based anticancer drug. *Bioorg Chem* 2019; **88**: 102925.

8 d'Amato TA, Landreneau RJ, McKenna RJ *et al.* Prevalence of in vitro extreme chemotherapy resistance in resected nonsmall-cell lung cancer. *Ann Thorac Surg* 2006; **81**: 440–6; discussion 6-7.

9 Vo JN, Cieslik M, Zhang Y *et al.* The landscape of circular RNA in cancer. *Cell* 2019; **176**: 869–81 e13.

10 Li J, Sun D, Pu WC, Wang J, Peng Y. Circular RNAs in cancer: Biogenesis, function, and clinical significance. *Trends Cancer* 2020; **6**: 319–36.

11 Memczak S, Jens M, Elefsinioti A *et al.* Circular RNAs are a large class of animal RNAs with regulatory potency. *Nature* 2013; **495**: 333–8.

12 Li C, Zhang L, Meng G *et al.* Circular RNAs: Pivotal molecular regulators and novel diagnostic and prognostic biomarkers in non-small cell lung cancer. *J Cancer Res Clin Oncol* 2019; **145**: 2875–89.

13 Zhang C, Ma L, Niu Y *et al.* Circular RNA in lung cancer research: Biogenesis, functions, and roles. *Int J Biol Sci* 2020; **16**: 803–14.

14 Chen Y, Wei S, Wang X, Zhu X, Han S. Progress in research on the role of circular RNAs in lung cancer. *World J Surg Oncol* 2018; **16**: 215.

15 Di X, Jin X, Li R *et al.* CircRNAs and lung cancer: Biomarkers and master regulators. *Life Sci* 2019; **220**: 177–85.

16 Zhong Y, Du Y, Yang X *et al.* Circular RNAs function as ceRNAs to regulate and control human cancer progression. *Mol Cancer* 2018; **17**: 79.

17 Cheng DL, Xiang YY, Ji LJ, Lu XJ. Competing endogenous RNA interplay in cancer: Mechanism, methodology, and perspectives. *Tumour Biol* 2015; **36**: 479–88.

18 Pastuszak-Lewandoska D, Kordiak J, Czarnecka KH *et al.* Expression analysis of three miRNAs, miR-26a, miR-29b and miR-519d, in relation to MMP-2 expression level in non-small cell lung cancer patients: A pilot study. *Med Oncol* 2016; **33**: 96.

19 Jiang MM, Mai ZT, Wan SZ *et al.* Microarray profiles reveal that circular RNA hsa_circ_0007385 functions as an oncogene in non-small cell lung cancer tumorigenesis. *J Cancer Res Clin Oncol* 2018; **144**: 667–74.

20 Tripathi A, Shrinet K, Kumar A. HMGB1 protein as a novel target for cancer. *Toxicol Rep* 2019; **6**: 253–61.

21 Wu L, Yang L. The function and mechanism of HMGB1 in lung cancer and its potential therapeutic implications. *Oncol Lett* 2018; **15**: 6799–805.

22 Wu XJ, Chen YY, Gong CC, Pei DS. The role of high-mobility group protein box 1 in lung cancer. *J Cell Biochem* 2018; **119**: 6354–65.

23 Livak KJ, Schmittgen TD. Analysis of relative gene expression data using real-time quantitative PCR and the 2 (−Delta Delta C(T)) method. *Methods* 2001; **25**: 402–8.

24 Mu Y, Xie F, Huang Y *et al.* Circular RNA expression profile in peripheral whole blood of lung adenocarcinoma by high: Throughput sequencing. *Medicine (Baltimore)* 2019; **98**: e17601.

25 de Fraipont F, Gazzeri S, Cho WC, Eymin B. Circular RNAs and RNA splice variants as biomarkers for prognosis and therapeutic response in the liquid biopsies of lung cancer patients. *Front Genet* 2019; **10**: 390.

26 Jin M, Shi C, Yang C, Liu J, Huang G. Upregulated circRNA ARHGAP10 predicts an unfavorable prognosis in NSCLC through regulation of the miR-150-5p/GLUT-1 axis. *Mol Ther Nucleic Acids* 2019; **18**: 219–31.

27 Wang C, Tan S, Liu WR *et al.* RNA-Seq profiling of circular RNA in human lung adenocarcinoma and squamous cell carcinoma. *Mol Cancer* 2019; **18**: 134.

28 Dong L, Zheng J, Gao Y *et al.* The circular RNA NT5E promotes non-small cell lung cancer cell growth via sponging microRNA-134. *Aging (Albany NY)* 2020;**12**: 3936–49.

29 Wang Y, Xu R, Zhang D *et al.* Circ-ZKSCAN1 regulates FAM83A expression and inactivates MAPK signaling by targeting miR-330-5p to promote non-small cell lung cancer progression. *Transl Lung Cancer Res* 2019; **8**: 862–75.

30 Tong S, Circular RNA. SMARCA5 may serve as a tumor suppressor in non-small cell lung cancer. *J Clin Lab Anal* 2020; e23195.**34**: e23195

31 Dong Y, Xu T, Zhong S *et al.* Circ_0076305 regulates cisplatin resistance of non-small cell lung cancer via positively modulating STAT3 by sponging miR-296-5p. *Life Sci* 2019; **239**: 116984.

32 Huang MS, Liu JY, Xia XB *et al.* Hsa_circ_0001946 inhibits lung cancer progression and mediates cisplatin sensitivity in non-small cell lung cancer via the nucleotide excision repair signaling pathway. *Front Oncol* 2019; **9**: 508.

33 Ye X, Lv H. MicroRNA-519d-3p inhibits cell proliferation and migration by targeting TROAP in colorectal cancer. *Biomed Pharmacother* 2018; **105**: 879–86.

34 Jin Y, Li Y, Wang X, Yang Y. Dysregulation of MiR-519d affects oral squamous cell carcinoma invasion and metastasis by targeting MMP3. *J Cancer* 2019; **10**: 2720–34.

35 Liang J, Liu Y, Zhang L, Tan J, Li E, Li F. Overexpression of microRNA-519d-3p suppressed the growth of pancreatic cancer cells by inhibiting ribosomal protein S15A-mediated Wnt/beta-catenin signaling. *Chem Biol Interact* 2019; **304**: 1–9.

36 Bai Y, Lu C, Zhang G *et al.* Overexpression of miR-519d in lung adenocarcinoma inhibits cell proliferation and invasion via the association of eIF4H. *Tumour Biol* 2017; **39**: 1010428317694566.

37 Wei B, Kong W, Mou X, Wang S. Comprehensive analysis of tumor immune infiltration associated with endogenous competitive RNA networks in lung adenocarcinoma. *Pathol Res Pract* 2019; **215**: 159–70.

38 Su X, Wang B, Wang Y, Wang B. Inhibition of TRIM32 induced by miR-519d increases the sensitivity of colorectal cancer cells to cisplatin. *Onco Targets Ther* 2020; **13**: 277–89.

39 Xie Q, Wang S, Zhao Y, Zhang Z, Qin C, Yang X. MiR-519d impedes cisplatin-resistance in breast cancer stem cells by down-regulating the expression of MCL-1. *Oncotarget* 2017; **8**: 22003–13.

40 Pang Y, Mao H, Shen L, Zhao Z, Liu R, Liu P. MiR-519d represses ovarian cancer cell proliferation and enhances cisplatin-mediated cytotoxicity in vitro by targeting XIAP. *Onco Targets Ther* 2014; **7**: 587–97.

41 Feng A, Tu Z, Yin B. The effect of HMGB1 on the clinicopathological and prognostic features of non-small cell lung cancer. *Oncotarget* 2016; **7**: 20507–19.

42 Ma Y, Kang S, Wu X, Han B, Jin Z, Guo Z. Up-regulated HMGB1 in the pleural effusion of non-small cell lung cancer (NSCLC) patients reduces the chemosensitivity of NSCLC cells. *Tumori* 2018; **104**: 338–43.

43 Jakubowska K, Naumnik W, Niklinska W *et al.* Clinical significance of HMGB-1 and TGF-beta level in serum and BALF of advanced non-small cell lung cancer. *Adv Exp Med Biol* 2015; **852**: 49–58.

44 Lv X, Yao L, Nie YQ, Xu XY. MicroRNA-520a-3p suppresses non-small-cell lung carcinoma by inhibition of high mobility group box 1 (HMGB1). *Eur Rev Med Pharmacol Sci* 2018; **22**: 1700–8.

45 Wu D, Liu J, Chen J, He H, Ma H, Lv X. miR-449a suppresses tumor growth, migration, and invasion in non-small cell lung cancer by targeting a HMGB1-mediated NF-kappaB signaling pathway. *Oncol Res* 2019; **27**: 227–35.

46 Liu PL, Liu WL, Chang JM *et al.* MicroRNA-200c inhibits epithelial-mesenchymal transition, invasion, and migration of lung cancer by targeting HMGB1. *PLOS One* 2017; **12**: e0180844.

47 Zheng H, Chen JN, Yu X *et al.* HMGB1 enhances drug resistance and promotes in vivo tumor growth of lung cancer cells. *DNA Cell Biol* 2016; **35**: 622–7.

48 Zhang R, Li Y, Wang Z, Chen L, Dong X, Nie X. Interference with HMGB1 increases the sensitivity to chemotherapy drugs by inhibiting HMGB1-mediated cell autophagy and inducing cell apoptosis. *Tumour Biol* 2015; **36**: 8585–92.

49 Jiao P, Hou J, Yao M, Wu J, Ren G. SNHG14 silencing suppresses the progression and promotes cisplatin sensitivity in non-small cell lung cancer. *Biomed Pharmacother* 2019; **117**: 109164.